


# Polycaprolactone/Gelatin/Hydroxyapatite Electrospun Nanomembrane Materials Incorporated with Different Proportions of Attapulgitte Synergistically Promote Bone Formation

Jun Liu<sup>1,2,\*</sup>, Siyu Wu<sup>1,2,\*</sup>, Jiayi Ma<sup>1,2</sup>, Chun Liu<sup>1</sup>, Ting Dai<sup>1</sup>, Xiaoyu Wu<sup>1</sup>, Hongbin Zhao<sup>1</sup>, Dong Zhou<sup>1</sup> 

<sup>1</sup>Medical Research Centre, The Affiliated Changzhou No.2 People's Hospital of Nanjing Medical University, Changzhou, 213164, People's Republic of China; <sup>2</sup>Dalian Medical University, Dalian, 116044, People's Republic of China

\*These authors contributed equally to this work

Correspondence: Hongbin Zhao; Dong Zhou, Medical Research Centre, The Affiliated Changzhou No.2 People's Hospital of Nanjing Medical University, Changzhou, 213164, People's Republic of China, Tel/Fax +86 13919761032; Tel/Fax +86 13861298585, Email zhao761032@163.com; zhoudong1012@163.com

**Purpose:** To enhance the osteoinductive effect of Hydroxyapatite (HA) in bone tissue engineering, this study manufactured polycaprolactone (PCL)/gelatin (GEL)/HA nanofibrous scaffolds incorporated with different ratios of attapulgitte (ATP): HA (0:3, 0:0, 1:1, 2:1 and 3:0) by high-voltage electrospinning. The synergistic effect exerted by ATP and HA on bone formation was explored both in vivo and in vitro.

**Methods and Results:** First, we determined the group composition and crystal structure of the nanosheets by Fourier transform infrared (FTIR) and X-ray diffraction (XRD) analyses. Then, the physical properties of the scaffolds, including the modulus of elasticity, porosity and water absorption were evaluated. Moreover, the surface microstructure of the nanofibrous scaffolds was captured by Scanning electron microscopy (SEM) and Transmission Electron Microscope (TEM). The biocompatibility of the fabricated scaffolds represented by cell counting kit 8 (CCK-8) and phalloidin staining was also assessed. Next, in vitro osteogenesis was evaluated. Real-time PCR, alkaline phosphatase (ALP) staining and Alizarin red S (ARS) staining results showed that the materials incorporated with HA and ATP at a ratio of 2:1 synergistically promoted more osteoblastic differentiation and extracellular mineralization than scaffolds doped with HA and ATP alone. Last, in vivo, Hematoxylin-Eosin staining (HE staining) and Masson staining showed that groups treated with HA and ATP acquired optimal patterns of bone regeneration.

**Conclusion:** This study clarified for the first time that the combination of HA and ATP orchestrated biomaterial-induced osseointegration, and the synergistic effect was more significant when the ratio of ATP/HA was 2:1. This conclusion also provides new ideas and a scientific basis for the development of functionalized nanomaterials in bone tissue engineering.

**Keywords:** attapulgitte, hydroxyapatite, bone regeneration, electrospinning technology

## Introduction

In current clinical practice, many large-scale bone injuries are caused by tumors, traumas, infections and other reasons.<sup>1</sup> Autologous bone grafting is the gold standard for the treatment of bone defects. However, the methods are relatively limited for these large-scale defects and a series of specific cases, such as autoimmune disease, bone infection, tumors, and insufficient bone mass.<sup>2,3</sup> Therefore, new treatment methods are urgently needed to address these serious bone injuries.<sup>4,5</sup>

In recent years, bone tissue engineering (BTE) has played an increasingly important role in the reconstruction and treatment of bone defects.<sup>6</sup> BTE is an organic combination of cells, growth factors, and struts, which are necessary in

hard tissue reconstruction to provide solid support of the defect site, accommodation for recruiting cells, and a micromilieu for metabolic waste/nutrient exchange. Bone substitutes, theoretical scaffolds to successfully rebuild BTE, are not only required to mimic the structural characteristics of the natural bone tissue matrix but are also supposed to have good biocompatibility, high osteoinductivity/conductivity, and appropriate biodegradation that match tissue ingrowth.<sup>7,8</sup>

In recent years, numerous strategies have emerged in which dozens of advanced technologies have been applied to manufacture bone substitutes in BTE.<sup>9–11</sup> Among these approaches, electrospinning technology is one of the most extensively used methods to produce continuous nanofibers ranging from microns to nanometers. Compared with techniques such as solvent casting, freeze drying, selective laser sintering and 3D printing, electrospinning technology is simply operated, relatively economical, and accessible all the time.<sup>12–16</sup> However, sometimes a single polymer ingredient cannot meet the mechanical strength, hydrophilicity and degradation rate requirements of a perfect biomaterial at the same time; therefore, the incorporation of several ingredients to form a composite can improve the performance of the ultimately synthesized biomaterial.<sup>17,18</sup> Gelatin (GEL), as a hydrophilic macromolecular colloid, is derived from the degradation product of collagen and is almost nonimmunogenic with host tissues. Moreover, gelatin retains the arginine-glycine-aspartic acid (RGD) sequence of collagen, which can promote cell adhesion, differentiation and proliferation.<sup>19–21</sup> However, its mechanical properties are not strong enough, and it degrades quickly, which hinders its application in BTE. In addition, polycaprolactone (PCL) has intense biomechanical properties, high histocompatibility, and relatively slow degradation, characteristics that make it a potentially supplementary component for GEL to construct an implant complex. Furthermore, it has been reported that the combination of PCL/GEL has significantly enhanced biomechanical intensity and can promote cell adhesion and proliferation, indicating the integration of these two ingredients.<sup>22</sup>

The biofunctions and properties of nanostructured materials can be modified by adjusting the electrospinning parameters, including the voltage applied and the nozzle diameter, conjugating bioactive agents, and adding specific functionalized coatings to enhance stem cell adhesion, infiltration, and differentiation and modulate the immunomicroenvironment, antitumor recurrence, and anti-infection expansion *in situ*.<sup>23,24</sup> Hydroxyapatite (HA), a natural inorganic component existing in bone, is widely applied in BTE due to its high bioaffinity and osteoinductivity/conductivity.<sup>25</sup> For example, Nilza Ribeiro's research on skin regeneration and repair confirmed that the calcium ions provided by nanohydroxyapatite significantly increased the growth and proliferation rates of human fibroblasts and human mesenchymal stem cells, preventing the adhesion of pathogenic strains commonly found in human skin flora.<sup>26</sup> However, its brittleness and low mechanical properties have limited its application.<sup>27,28</sup> Jong Ho Lee's study reported that osteoblast proliferation and differentiation are very low in the presence of HAp compared to other bone substitutes, although hydroxyapatite could accelerate new bone deposition.<sup>29,30</sup> In addition, attapulgite (ATP) is a type of hydrated silicate with a porous structure and structural formula of  $(Al_2Mg_2)Si_8O_{20}(OH)_2(OH_2)_4 \cdot 4H_2O$ . ATP is usually employed as an adsorbent, decolorizer and catalyst in the environmental industry because of its high adhesion, surface area and water absorption, and many studies have proven that it has bone bioactivity both *in vitro* and *in vivo*.<sup>31–34</sup> In this study, we fabricated PCL/GEL nanofibrous scaffolds by electrospinning, and different proportions of HA and ATP were added to the prepared scaffolds to explore whether the combination of ATP and HA is capable of exerting a synergistic osteogenic effect and potentiating bone regeneration after large defects.

## Materials and Methods

### Materials

PCL (Mw, 80,000) was purchased from Aladdin Reagents LTD. Gelatin (Gel, ~250 g Bloom, Aladdin Chemical Inc., Shanghai, China), hexafluoro-isopropyl alcohol and hydroxyapatite (Mw, 502.31; <100 nm particle size) were purchased from Shanghai Aladdin Biochemical Technology. Attapulgite (150–500 nm) was provided by the Lanzhou Institute of Chemical Physics, Chinese Academy of Sciences. Dulbecco's-modified Eagle's medium (DMEM basic, Gibco, Thermo-Fisher Biochemical Products, Beijing, China) was supplemented with 5% v/v fetal bovine serum (FBS, Biological Industries, Israel) and 1% v/v penicillin/streptomycin (Life Technologies Corporation, USA) for the complete medium for use with BMSCs.

## Preparation of PCL/GEL/ATP/HA Electrospinning Nanomaterials

Gelatin (0.67 g) and PCL (1.33 g) were added to 20 mL hexafluoro-isopropanol solution under constant stirring at room temperature. Then, ATP/HA in different proportions (0:0, 0:3, 1:1, 2:1, 3:0) was added after the PCL/GEL mixture became homogenous. Finally, a uniform mixed solution of 30 wt% ATP/HA was obtained. Then, the solution was added into the propeller and installed in the propulsion system. The propulsion speed was adjusted to 0.0050 cm/s, and the voltage was stabilized at 20 kV. A flat 20 mm needle was used, and the 16 cm distance between the needle tip and the plate was covered with aluminum foil. After finishing spraying, the nanosheets were placed into the oven at 37 °C overnight to remove any possibly remaining solvent and stored at 4 °C. Pristine PCL/GEL nanostructured scaffolds were referred to as the PG group, PCL/GEL nanostructured scaffolds contained ATP alone, HA alone, ATP/HA (2:1) and ATP/HA (1:1) were named the PG-A, PG-H, PG-A2H1 and PG-A1H1 groups, respectively.

## Morphology and Characterization of the Composite Nanofibrous Scaffold

### Scanning Electron Microscopy (SEM) and Transmission Electron Microscope (TEM)

The nanofibrous materials were cut into a square with a size of 1 cm × 1 cm and uniform thickness. After drying, the materials were fixed on a copper column and sprayed with Pt powder on the surface of the material for 1 hour. Scanning electron microscopy was used to observe the surface morphology and microstructure of the nanofibers, meanwhile, Energy Dispersive Spectrometer (EDS) was used to observe the elemental composition. The distribution and diameter of nanofibers and the pore size were measured by ImageJ software (National Institutes of Health, USA). TEM images captured by a high-resolution transmission electron microscope (Tecnai G2 F20, FEI, USA) after the nano-ATP powder was dispersed in anhydrous ethanol by sonication and dropped onto a micro grid.

### XRD Patterns and FTIR Analysis

X-ray diffraction (XRD) patterns of scaffolds from each group were collected with an X'Pert PRO diffractometer (XRD, X'Pert-MPD, Philips, Holland) in a fixed time mode at a stepping interval of approximately 0.167°.

Fourier transform infrared (FTIR) spectroscopy was used to measure the functional group composition of nanomaterials. PCL/GEL/ATP/HA electrospun films were cut into samples with a size of 1 cm × 1 cm and loaded onto a Nicolette NEXUS spectrometer with a resolution of 4 cm<sup>-1</sup>. Each sample was scanned three times to obtain spectral results ranging from 400 to 4000 cm<sup>-1</sup>.

### Swelling Rate and Porosity Measurement

Swelling rate: Three samples from each group were cut into square nanofilms with a size of 2 cm × 2 cm, and the thickness was controlled at approximately 1 mm. The samples were soaked in distilled water at 37 °C for 4, 8, 12, 16 and 24 hours. At each timepoint, samples were extracted, dried and weighed again, and the swelling rate was calculated as follows:

$$\text{Swelling}(\%) = \frac{W_2 - W_1}{W_1} \times 100\%$$

where W1 is the initial weight of the material and W2 is the weight of the material after soaking in distilled water.

Porosity: A certain volume (30 mL, V1) of ethanol was added to the measuring cylinder, and the total volume (V2) was measured after the nanometer film material was fully infiltrated. After 24 hours, the ethanol-containing material was discarded, and the volume of the remaining ethanol in the measuring cylinder (V3) was measured. The porosity of the material was calculated using the following formula:

$$\text{Porosity}(\%) = \frac{V_1 - V_3}{V_2 - V_3} \times 100\%$$

### Evaluation of Degradation

All samples were freeze-dried before the in vitro degradation evaluation and weighed (W0). Then, these samples were soaked in PBS (0.1 M, pH = 7.4) solution at 37 °C for 1, 2, 3, 4, 5, and 6 weeks and other different time periods. At each

time point, the samples were taken out, freeze-dried, and weighed (W1). The measurement was repeated 3 times. The weight loss was calculated using the following formula:

$$\text{Degredation}(\%) = \frac{W1 - W0}{W0} \times 100\%$$

### Water Contact Angle Analysis

The hydrophilicity of nanosheets was determined by the OCA-20 Contact Angle system (Data physics Instruments, Filderstadt, Germany). The sheets from each group were placed on a test board, and 0.01 mL of deionized water was dropped onto the surface of the tested sample. After 10s, the water contact angle (WCA) was recorded by a video monitor. These tests were repeated three times ( $n = 3$ ).

### Mechanical Performance Test

The nanosheets were trimmed to a length of 6 cm and a width of 1 cm, and the mechanical properties of the nanofiber membranes were tested under dry and wet conditions (samples were soaked in PBS for 24 hours). An MTS 4204 universal testing machine (MTS system (China) Co., LTD, China) was used for tensile performance testing. In brief, the two ends of the test sample were equipped with a 20 kN load cell and inserted between two clamps exposing a surface area of 4 cm<sup>2</sup>. The upper clamp was raised at a 10 mm/min crosshead speed until the breaking point, and a stress–strain curve was obtained. Stress–strain was applied to analyze the Young's modulus (E), ultimate tensile strength (UT) and elongation at break of the nanomembranes.

### Thermogravimetric Analysis

A TGA analyzer (TG 209 F3, Tarsus, Netzsch, Germany) was used to test the thermogravimetry of the electrospun nanomembrane. Samples from each group weighing  $10 \pm 0.1$  mg were placed on a platinum pan for thermal analysis and then heated at 30 °C with an increasing temperature of 10 °C/min up to 1000 °C. The analysis was performed under a nitrogen atmosphere with a flow rate of 100 mL/min. In TG analysis, the relative sample weight was continuously recorded with a mass accuracy of  $\pm 0.1\%$ .

### AFM Measurement

The tapping mode of the atomic force microscope (NanoWizard II AFM, Berlin, Germany) was used to analyze the surface roughness of the electrospun membrane. The measurement was performed after placing the sample on the scanning surface, and all conditions were kept the same: the scan rate and scan size were 1 Hz and  $15 \times 15$  μm, respectively.

## In vitro Biocompatibility

### Extract Preparation and Cell Proliferation

Extracts of PCL/GEL/ATP/HA nanofilms were collected after these nanofilms (thickness  $\leq 1$  mm) were soaked in DMEM at a ratio of 3 cm<sup>2</sup>/mL for 24 hours in accordance with the protocol of the Chinese National Standard (GB/T 169886.12). Afterward, the extracts were filtered with a 0.22 μm strainer and stored. Mouse-sourced bone mesenchymal stem cells (BMSCs) were acquired from ATCC (ATCC, CRL-12424) and incubated at 37 °C and 5% CO<sub>2</sub>.

The proliferation of BMSCs affected by nanofilms was evaluated by a cell counting kit 8 (CCK-8, Dojindo Kagaku, Japan). BMSCs were inoculated in 96-well plates at a density of  $4 \times 10^3$  cells/well. After the cells attached, the medium was switched to nanofilm extracts from each group. At 1, 3, and 5 days after incubation, CCK-8 tests were carried out according to the manufacturer's instructions. Finally, a microplate reader was used to detect the absorbance at a wavelength of 450 nm in the wells of 96-well plates.

### Morphological Structure of Cell Culture on the Material

BMSCs were inoculated on  $2 \times 2$  cm<sup>2</sup> nanofilm in a six-well plate ( $1.6 \times 10^5$  cells/well) for 3 days. After that, scaffolds with adherent cells were fixed for 30 minutes with 4% glutaraldehyde. Then, the nanofilms were dehydrated in a serial

gradient alcohol solution (75%, 80%, 90% and 100%). Subsequently, they were freeze-dried in a vacuum lyophilizer for 24 h. The morphology of the adherent cells was examined by SEM.

### Cytoskeleton Actin Staining and LIVE/DEAD Staining

BMSCs were seeded on the surface of sterilized nanosheets (Go60 irradiation) in a 6-well plate ( $1.6 \times 10^5$  cells/well). Then, the nanosheets were treated with 0.01% Triton X-100 for 10 min of cell membrane permeabilization. After washing with PBS 3 times, staining with 1 mL phalloidin (50  $\mu\text{g}/\text{mL}$ ) (Yeasen, Shanghai, China) for 30 min, and counterstaining with 1 mL DAPI (5  $\mu\text{g}/\text{mL}$ ) (Dojindo Laboratories, Kumamoto, Japan) solution, the images of cells spreading out on the nanosheets were observed under a fluorescence microscope (IX71-22FL/P, Olympus, Japan).

Cell viability was evaluated using a LIVE/DEAD staining kit (L-7011; Invitrogen, Eugene, OR, USA). The cells were cultured with the extract solution for 3 days, and 600  $\mu\text{L}$  of LIVE/DEAD reagent was added to each well. The images were observed under a fluorescence microscope (IX71-22FL/P, Olympus, Japan). The red fluorescence and green fluorescence represent dead cells and live cells, respectively.

## Osteogenesis Evaluation

### Alizarin Red S Staining and Alkaline Phosphatase (ALP) Staining

BMSCs were seeded in a 12-well plate at a density of  $2 \times 10^4$  cells/ $\text{cm}^2$ . Then, extracts of the PCL/GEL/ATP/HA nanomembrane were exchanged for cell culture to induce osteogenesis. Calcium deposits were detected using an Alizarin Red S Staining kit. After 14 days of cell culture, the culture medium was removed and washed with PBS 2–3 times, followed by fixation with 4% paraformaldehyde at 37 °C for 15 min and then staining with 1% (W/V) Alizarin Red S solution for 45 min. Finally, the samples were washed again with PBS (0.1 M, pH = 7.4) and observed directly under an optical microscope.

Similarly, after coculturing BMSCs with extracts for 14 days, BCIP/NBP reagent (Beyotime, China) was applied to visualize ALP activity, and the samples were also observed under an optical microscope.

### Expression Level of Osteogenic Genes Detected by Real-Time PCR (RT-PCR)

To evaluate the osteogenic properties of nanostructured scaffolds incorporated with HA, ATP, and both combined, BMSCs were seeded on nanostructured scaffolds in a 6-well plate. At each timepoint (1, 3, and 7 days), total RNA was extracted using a NucleoZol kit (Macherey-Nagel, Germany) according to the instructions. After that, reverse transcription was carried out to synthesize cDNA using the HiScript II Q RT SuperMix reagent Kit (Vazyme, China). Then, gene amplification was performed using the SYBR Premix Ex Taq-TM Real-time PCR kit (Vazyme, China), and the osteogenesis-related primers (alkaline phosphatase (*ALP*), osteocalcin (*OCN*), osteopontin (*OPN*), Osterix (*OSX*), and Runt-related factor 2 (*Runx2*) used in this study are listed in Table 1.

**Table 1** Primer Sequences Applied to RT-PCR Analysis

Gene	Forward Primer	Reverse Primer
<b>GAPDH</b>	5'-CACCACCAACTGCTTAGC-3'	5'-TTCACCACCTTCTTGATGTC-3'
<b>ALP</b>	5'-GCAGTATGAATTGAATCGGAACAAC-3'	5'-ATGGCCTGGTCCATCTCCAC-3'
<b>OPN</b>	5'-TACGACCATGAGATTGGCAGTGA-3'	5'-TATAGGATCTGGGTGCAGGCTGTAA-3'
<b>Runx2</b>	5'-CTGCAAGCAGTATTTACAACAGAGG-3'	5'-GGCTCACGTCGCTCATCTT-3'
<b>OSX</b>	5'-AGGCCTTTGCCAGTGCCTA-3'	5'-GCCAGATGGAAGCTGTGAAGA-3'

**Abbreviations:** GAPDH, glyceraldehyde-3-phosphate dehydrogenase; ALP, alkaline phosphatase; OPN, osteopontin; OSX, osterix; Runx2, runt-related transcription factor 2.

## In vivo Evaluations

### Study of Skull Defect Repair in Rats

To explore the synergistic osteogenic effect of nanostructured scaffolds incorporated with ATP/HA *in vivo*. We used a 5 mm rat skull defect model. In brief, 15 male SD rats (4 weeks old, 150 g/rat) were used in the study. All rats were anesthetized by intraperitoneal injection of 3% pentobarbital (100 mg/kg). Then, the rat scalp was disinfected, a 1.8 cm incision was made in the middle of the scalp, the soft tissue was carefully separated to expose the cranium, and two 5 mm symmetrical cylinder defects were drilled. The bone fragments were washed with normal saline and implanted with nanostructured scaffolds. Then, the soft tissue and skin were sutured layer by layer. Four million U of penicillin was injected daily for seven consecutive days to prevent postoperative infection. At 12 weeks after the operation, the rats were sacrificed with pentobarbital, and the skull specimens were removed. The soft tissues around the skull were kept and fixed with 10% formalin for subsequent evaluation. All experimental protocols were approved by the Animal Research Committee of the Affiliated Changzhou No.2 People's Hospital of Nanjing Medical University. The animal experiments comply with Animal Care and Use Committee (IACUC) guidelines.

### Histological and Immunohistochemical Staining

The skull samples were demineralized with 15% EDTA (37 °C, pH = 7.0) for 6 weeks, dewaxed with serial gradient ethanol, embedded in paraffin, and then sectioned into 5- $\mu$ m-thick slices. Histological staining (H&E staining, Masson's trichrome (MT) staining and Van Gieson staining) was performed, and the staining results were observed under an optical microscope (Olympus, Japan). The percentage of new bone area relative to defect area was assessed using Image-Pro Plus 6.0 software (Media Cybernetics, Rockville, MD, USA).

To detect osteogenesis-related protein expression *in vivo*, immunohistochemical staining was performed. Briefly, after the slices were dewaxed, they were permeabilized with 5% Triton X-100 and blocked with 5% BSA solution. Mouse monoclonal antibodies against Col-1 (1:200, Abcam, USA), Runx2, OCN (1:200 dilution, Santa Cruz, USA) and OPN (1:100, Abcam, Britain) were employed to detect the corresponding antigens overnight at 4 °C. Then, the slices were treated with biotinylated goat anti-mouse secondary antibody and SABC for 30 minutes at 37 °C. Subsequently, sections were treated with 3,3'-diaminobenzidine tetrahydrochloride (DAB), counterstained with dehydrated hematoxylin, and observed by optical microscopy (Olympus, Japan).

### Statistical Analysis

Data in this study are presented as the mean  $\pm$  standard deviation, GraphPad Prism version 7.0 (San Diego, CA, USA) was used for data analysis. One-way analysis of variance (ANOVA) was used to determine statistical significance between groups.  $P < 0.05$  was considered statistically significant.

## Results

### Surface Morphology of Nanofiber Membranes

As shown in [Figure 1A](#), continuous nanofibers were observed in all groups, with no obvious difference in the surface microstructure of these fabricated nanoscaffolds. In general, these nanofibers largely ranged from 200  $\mu$ m to 900  $\mu$ m and were evenly distributed, forming pore structures. As the ATP content increased, the diameter of the nanofibers decreased slightly ([Figure 1B](#)). The roughness of the scaffold surface at the nanoscale was further observed by AFM ([Figure 1C](#)). As the proportion of ATP increased, the surface of the nanofiber membrane became rougher than other samples, especially the PG-A2H1 group, which had the toughest surface topology.

### Morphological Characteristics of ATP and Composition Analysis of Electrospun Nanofiber Membranes

The morphological characteristics of ATP at the microscale were measured by scanning electron microscopy (SEM) and transmission electron microscopy (TEM). ATP presents a rod-like crystal structure, and the length of the nanorods was approximately 300–500 nm with a diameter range from 15 to 50 nm ([Figure 2A](#) and [B](#)). [Figure S](#) shows the element content results of attapulgite, it can be seen that ATP is composed of elements such as Si, Mg, Al, Si, etc. To determine the

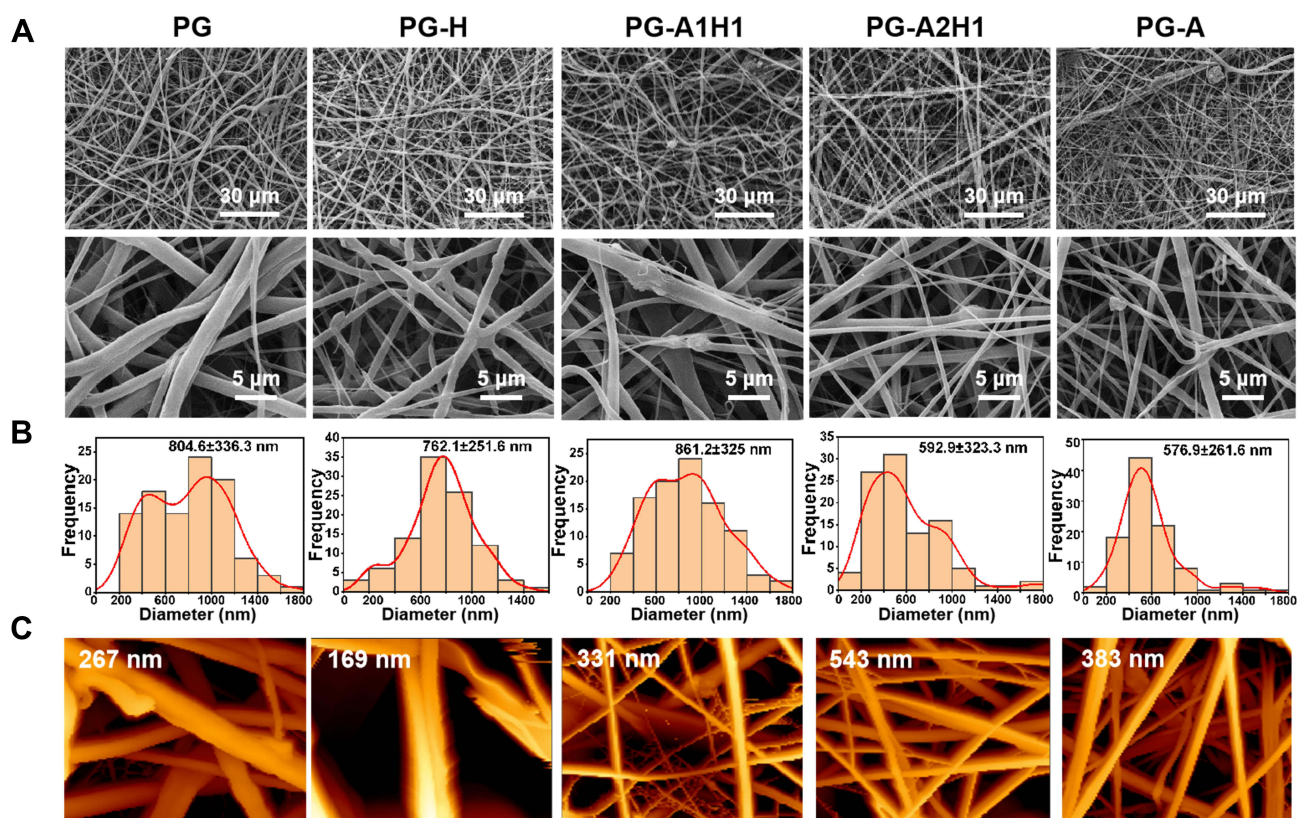


**Figure 1** The microstructures of the scaffold surfaces. **(A)** SEM images. **(B)** The diameter distributions of the nanofiber membranes. **(C)** AFM images of different nanomembranes. The diameters of the nanofiber are expressed as the mean  $\pm$  standard deviation.

**Abbreviations:** SEM, scanning electron microscopy; AFM, atomic force microscope.

composition of the scaffolds, FTIR (Figure 2C) and XRD (Figure 2D) analyses were carried out. The FTIR results show that the characteristic peaks of gelatin (amide 1,  $1650\text{ cm}^{-1}$  and amide 2,  $1540\text{ cm}^{-1}$ ) and the characteristic peaks of PCL (asymmetric  $-\text{CH}_2$  stretching and symmetric  $-\text{CH}_2$  stretching) appeared in all groups, indicating that each group of nanomembranes contains both gelatin and PCL. Moreover, with the change in the ratio of ATP and HA, the peak at  $350\text{ cm}^{-1}$  also changed correspondingly. In addition, XRD patterns clearly showed that the peaks of different groups changed correspondingly at  $8.4^\circ$  and  $31.7^\circ$  with the change in ATP/HA content (Figure 2D), which demonstrates that ATP and HA were successfully incorporated into the nanosheets. These results were also consistent with those of an earlier study.<sup>32</sup>

## Characterization of Nanofiber Membranes

Figure 2E shows the results of the thermal weight loss analysis of the nanofiber membrane. The mass loss of the nanomembrane mixed with different ratios of ATP/HA was lower than that of the PG group below  $450^\circ\text{C}$ , and PG-A2H1's mass loss was minimal among the groups. At  $900^\circ\text{C}$ , the mass loss of the PG-A1H1 group was the lowest, indicating that ATP increased the thermostability of the nanostructured scaffolds.

Figure 2F displays the water absorption rate of the nanomembranes. The water swelling rate increased after adding different proportions of ATP/HA and was the highest in the PG-A2H1 group. As shown in Figure 2I, the porosity of the different groups was no significant difference.

Figure 2G shows the in vitro degradation of scaffolds from each group for 6 weeks. All groups had a fast degradation rate at three weeks. The PG group degraded the fastest among all the groups. The PG-A2H1 group still had 84% of its initial mass at 6 weeks, while the PG group degraded the fastest and had approximately 78% of its initial mass remaining. In addition, the degradation rate of PG-A2H1 was slower than that of any other group after three weeks. Therefore, adding ATP could slow the degradation of the biomaterials.

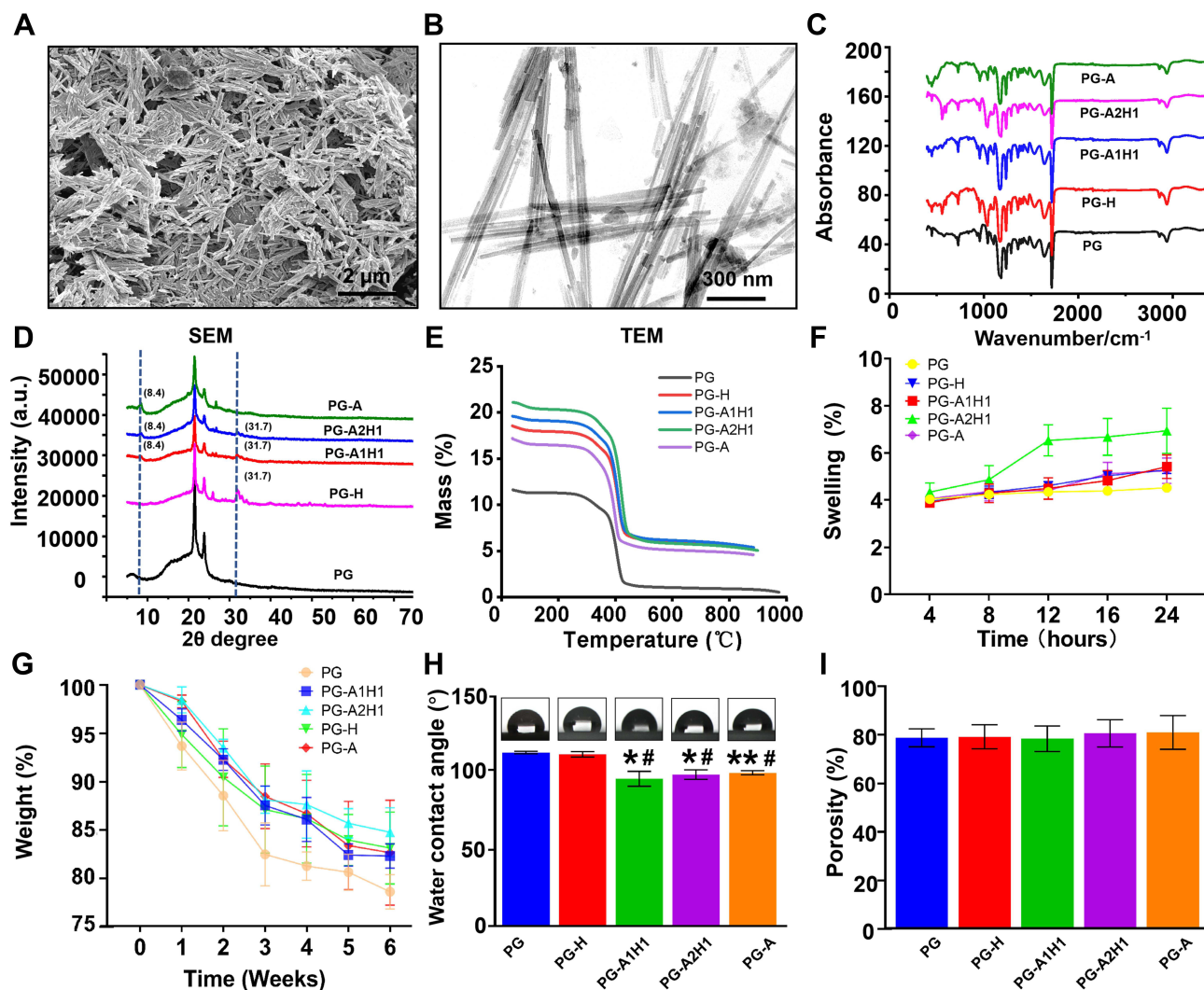


**Figure 2** Morphological characteristics and composition analysis of electrospun nanofiber membranes. (A) SEM image of nano-ATP. (B) TEM image of nano-ATP. (C) FTIR spectra. (D) XRD patterns. (E) TGA. (F) Swelling and (G) degradability of the scaffolds. (H) Water contact angle. (I) Porosity. Data are expressed as the mean  $\pm$  standard deviation. \* $p < 0.05$ , \*\* $p < 0.01$  compared to the PG group. # $p < 0.05$  compared to the PG-H group.

**Abbreviations:** SEM, scanning electron microscopy; nano-ATP, nano-attapulgite; TEM, transmission electron Microscope; FTIR, Fourier transform infrared spectroscopy; TGA, thermogravimetric analysis.

Figure 2H shows the water contact angle (WCA) results. Groups containing ATP exhibited decreased WCA compared with other groups, demonstrating that the hydrophilicity of the nanoscaffold was improved after integration with ATP.

Bone defect implantation requires good biomechanical properties of bone substitutes (Figure 3). Figure 3A and B depict the stress–strain curves of the biomaterials under dry and wet conditions. The elastic moduli of the control group were  $7.59 \pm 0.47$  MPa and  $14.97 \pm 0.58$  MPa in the dry state and wet states, respectively, which indicated that the modulus of elasticity improved under wet conditions. Moreover, the elastic modulus of the nanofibrous membranes improved with increasing attapulgite content in the dry state. However, the change was reversed under wet conditions (Figure 3C). The strain at break of the scaffolds decreased with increasing ATP in both the dry and wet states (Figure 3D). The tensile strength of attapulgite-added scaffolds was higher than the control group in the dry state; however, the tensile strengths of the PG-H and PG-A groups were lower than that of the control group in the wet condition (Figure 3E).

## Evaluation of Scaffold Biocompatibility

Figure 4A shows the cell attachment on scaffolds after 3 days of incubation as observed by SEM. The BMSCs adhered to the scaffolds from each group grew well, spread out evenly, and exhibited a favorable morphology. Moreover, Figure 4B



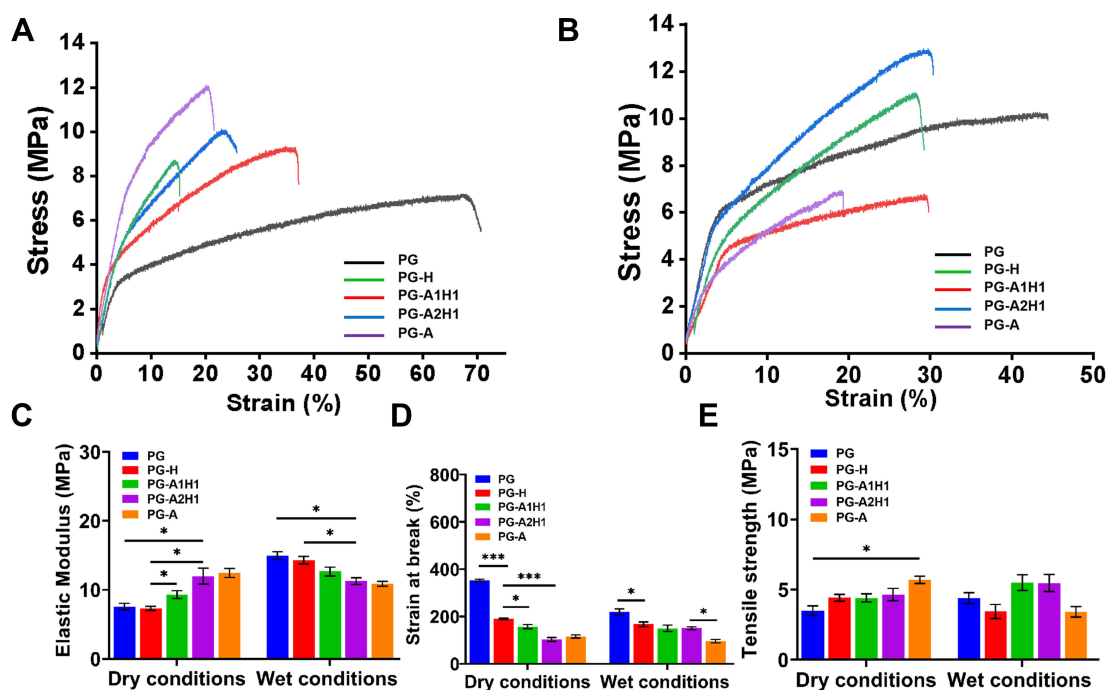


**Figure 3** Tensile properties of the nanofiber membrane. (A) Stress–strain curve (dry conditions), (B) Stress–strain curve (wet conditions), (C) Elastic modulus, (D) Strain at break, (E) Tensile strength. Data are expressed as the mean  $\pm$  standard deviation. \* $p < 0.05$ ; \*\*\* $p < 0.001$  between groups.

shows Live/dead-stained images of cells after coculture with the extract of scaffolds after 3 days. BMSCs in each group proliferated well, and few dead cells were observed. Figure 4C shows the cytoskeletal staining in which BMSC nuclei were stained with Hoechst (blue), and F-actin was stained with rhodamine phalloidin (green). After three days of adherence, BMSCs showed more outstretched filopodia-like extensions than the control group. These results demonstrated that BMSCs can adhere and proliferate well on the scaffolds, indicating that the nanomembranes possess favorable biocompatibility for BMSCs.

The cytotoxicity of the nanomembrane was tested by CCK-8 in vitro. Figure 4D shows that the proliferation of BMSCs was affected by the extracts of each group. At 1, 3, and 5 days, the groups incorporated with ATP had the same proliferation rate as the negative control group. Notably, the PG-A1H1 and PG-A2H1 groups had more proliferative effects on Day 5 than the control group (\* $p < 0.05$ ).

## Expression of Osteoblast Molecular Markers in in vitro Experiments and Evaluation of Osteogenic Induction Performance

Figures 5A–D show the expression of specific osteogenic molecular marker mRNAs, which were measured by quantitative real-time PCR assay (RT–qPCR). The gene expression levels of *ALP*, *OPN*, *OSX*, and *Runx2* were significantly upregulated after incorporating different proportions of ATP/HA in the scaffolds on Days 1, 3, and 7. *ALP* and *OPN* expression levels were increased in the PG-A1H1 group compared with the PG-H group on Day 1 (\* $p < 0.05$ ). The expression levels of *ALP* and *OSX* in the PG-A2H1 group were increased compared with those in the PG-H group after 3 days of culture (\*\*\* $p < 0.001$ ). On Day 7, the expression levels of *OPN* and *Runx2* in the PG-A1H1 groups were significantly higher than those in the PG and PG-H groups (\*\*\* $p < 0.001$ ).

BMSCs were cultured in the DMEM, control group and incorporated ATP/HA groups, which were cultured in their extract media for 14 days. Figure 5E shows the results of Alizarin Red S staining, which verified the mineralized calcium nodules, which were most prominent in the PG-A1H1 and PG-A2H1 groups compared with the control group and the pure HA group (PG-H). Figure 5F shows the results of ALP staining, which revealed that the groups that incorporated ATP had higher activity than the control group. Moreover, the staining gradually deepened after the attapulgit content increased.

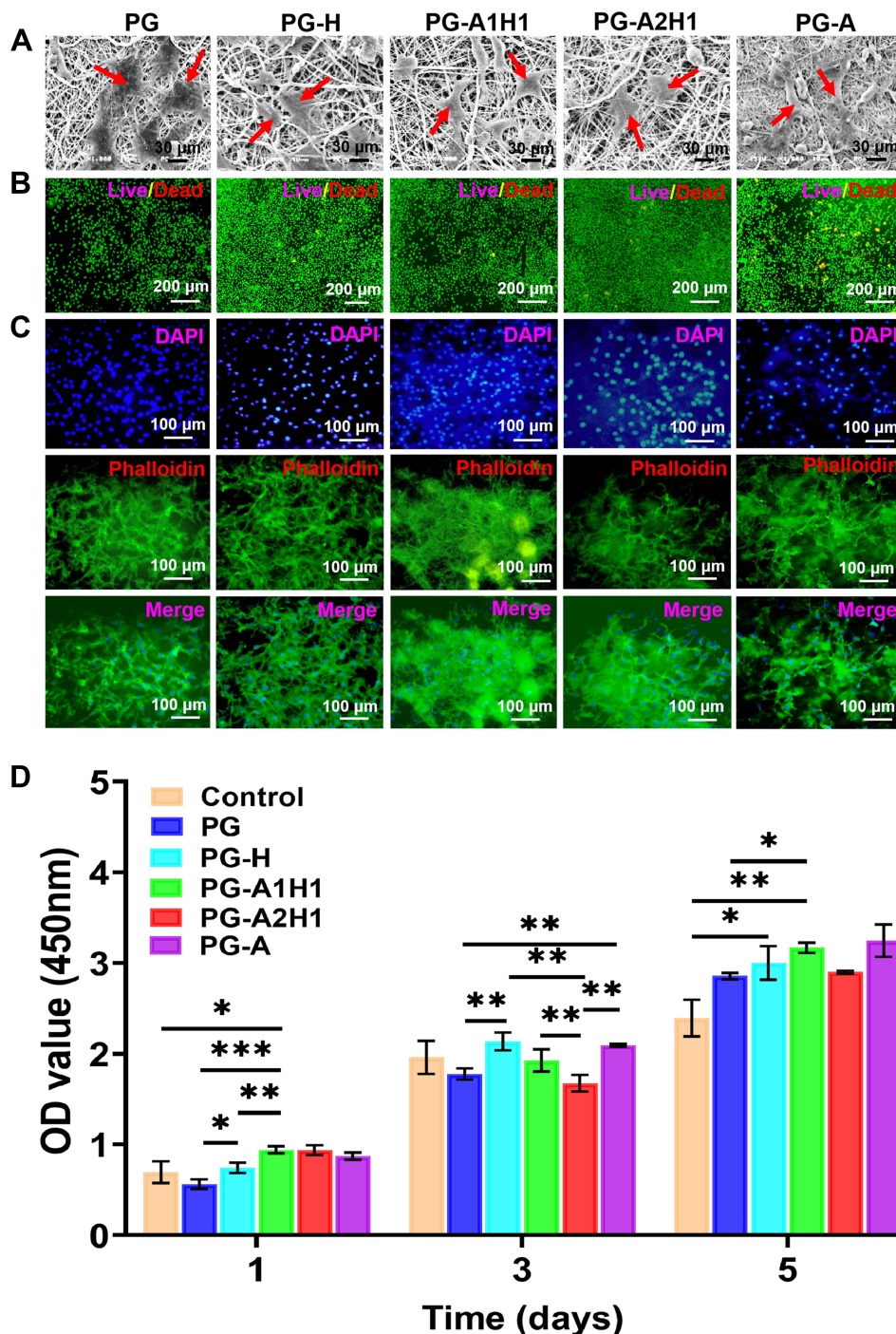


**Figure 4** In vitro biocompatibility of scaffolds. (A) SEM images of BMSCs seeded on the material for 3 days (scale bar = 30  $\mu$ m), the red arrows indicate BMSCs. (B) Live/dead staining after culturing BMSCs for 3 days on scaffolds, the living cells and dead cells are stained green and red, respectively (scale bar = 200  $\mu$ m). (C) The representative fluorescence images of BMSCs cultured on scaffolds at 3 days, cell nuclei were stained blue by DAPI and F-actin was stained green with phalloidin (scale bar = 100  $\mu$ m). (D) The viability of BMSCs cultured with extracts from different groups after 1, 3, and 5 days measured by CCK-8. Data are expressed as the mean  $\pm$  standard deviation. \* $p$  < 0.05; \*\* $p$  < 0.01; \*\*\* $p$  < 0.001 between groups.

**Abbreviations:** SEM, scanning electron microscopy; BMSCs, Mouse-sourced bone mesenchymal stem cells; CCK-8, cell counting kit-8.

## Histological Evaluation of Bone Regeneration

At 12 weeks after the operation, the rat skull tissue was removed, and the new bone tissue was evaluated after 2 months of decalcification. The results are shown in Figure 6A–D. In the control group, most of the bone defect area was still connective tissue, and there was no obvious new bone tissue growth. After mixing different proportions of the ATP/HA

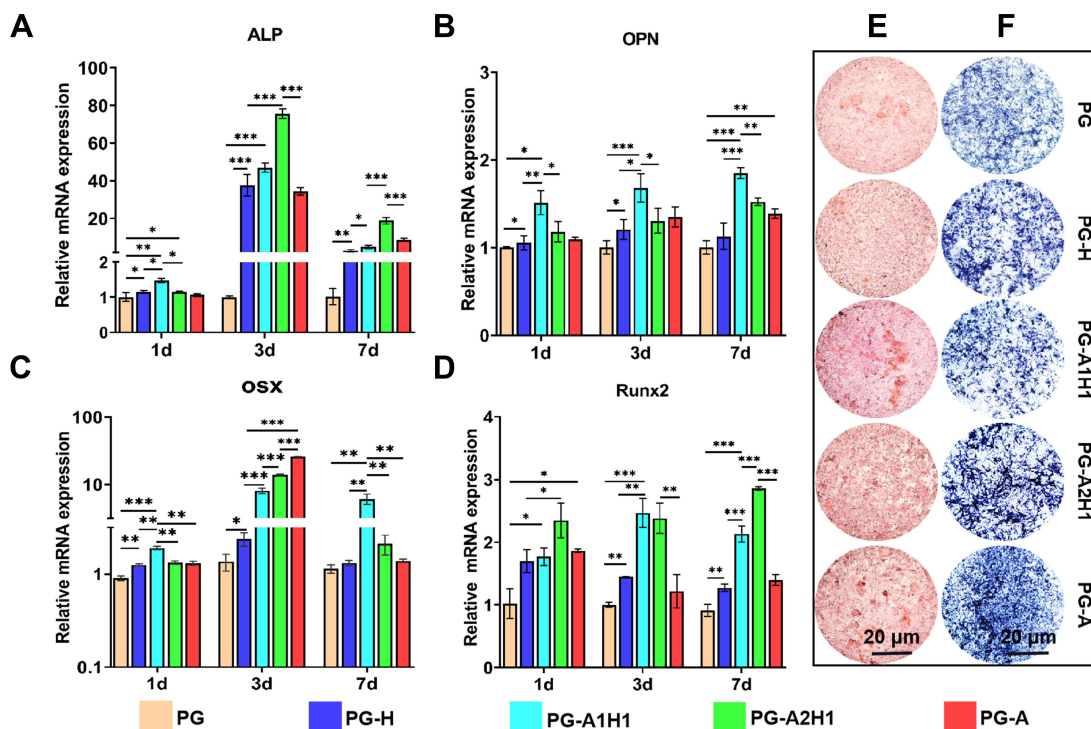


**Figure 5** Osteogenic gene expression and mineralization of different groups. (A–D) Expression of the osteogenic gene-specific markers at day 1, day 3, and day 7: (A) ALP, (B) OPN, (C) OSX, and (D) Runx2. (E) Alizarin Red S staining and (F) Alkaline phosphatase staining after 14 days of BMSCs cocultured with extracts (scale bar = 20 µm). Data are expressed as the mean ± standard deviation. \* $p < 0.05$ ; \*\* $p < 0.01$ ; \*\*\* $p < 0.001$  between groups.

**Abbreviations:** ALP, alkaline phosphatase; OPN, osteopontin; OSX, osterix; Runx2, runt-related transcription factor 2.

materials, new bone tissue growth was observed at the edge of the scaffolds. Masson staining (Figure 6A) revealed blue-stained collagen fiber tissues in the pores of the nanomembrane material, and as the ratio of different groups of ATP/HA changed, the area of new bone tissue also changed. While changes occurred there, the area of new bone tissue was the most significant in the PG-A1H1 and PG-A2H1 groups.

## Immunohistochemical Evaluations

Twelve weeks after planting, immunohistochemical (IHC) staining was performed (Figures 7A–D and 8A–D). Runx2, OCN, OPN, and Col-1 were expressed to varying degrees in each group, and when the ATP/HA content gradually increased, their expression levels showed a tendency to increase first and then decrease, indicating that the expression levels of osteogenic-related proteins were affected by the dynamic change in the ATP/HA ratio. The protein expression levels of Runx2, OCN, OPN, and Col-1 were significantly increased in the PG-A1H1 and PG-A2H1 groups. The expression levels of Col-1 and OPN in the PG-A1H1 group were higher than those in the PG-H group (\* $p < 0.05$ ), indicating that ATP can enhance the role of hydroxyapatite in the direction of osteogenic induction, and there is a certain relationship between the enhancement effect and its ratio.

## Discussion

HA is the primary inorganic component in bone tissue and has biocompatibility, bioactivity and osteoconductivity; therefore, synthesized hydroxyapatite has been broadly used in tissue engineering applications, such as bone transplantation and drug carriers.<sup>35</sup> However, the effects of hydroxyapatite on BMSC differentiation and osteogenic induction are weak.<sup>29</sup> Moreover, its brittleness and low fracture toughness have limited its application.<sup>36,37</sup> By incorporating different trace elements, such as magnesium, zinc, and strontium, and incorporating other materials, the scaffolds' physicochemical properties and osteogenic effects can be enhanced.<sup>38</sup> Shiao-Wen Tsai's acquired strontium-substituted hydroxyapatite nanofiber (Sr-HANF) matrices were fabricated by electrospinning, which proved that HA-incorporated Sr

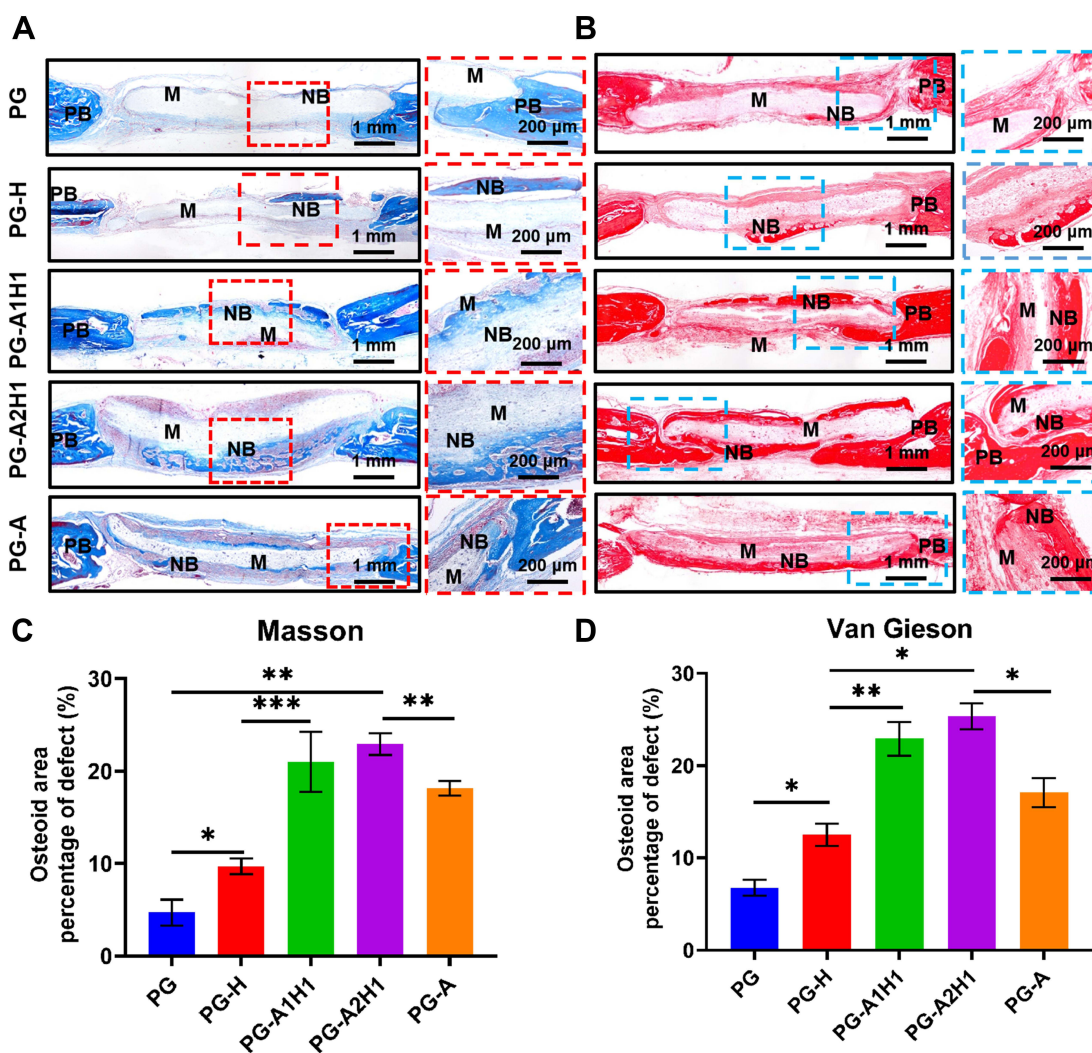


**Figure 6** Histological staining results of electrospun nanofibrous membranes with different ratios of ATP and HA after 12 weeks of implantation in rat skull defects. **(A)** Masson Staining. **(B)** Van Gieson staining. **(C and D)** Quantitative analysis of **(A and B)**. Scale bars = 1 mm or 200  $\mu\text{m}$ . \*  $p < 0.05$ , \*\*  $p < 0.01$ , \*\*\*  $p < 0.001$  between groups. **Abbreviations:** PB, primitive bone tissue; M, material; NB, new bone.

ions could enhance the differentiation of MG63 osteoblast-like cells.<sup>39</sup> Therefore, combining hydroxyapatite with other materials to improve its physicochemical properties and osteoinductive effects has become a potential research direction.<sup>28</sup> In the process of this research, we successfully acquired PCL/GEL nanostructured scaffolds doped with nano-ATP and HA in different proportions for bone tissue engineering by using electrospinning technology.

After adding different contents of ATP/HA, the diameter of the nanofibers was reduced, which could be because the incorporation of ATP/HA increased the charge density of the solution. Son et al's approach indicated that the addition of cationic and anionic polyelectrolytes could enhance the conductivity of the solution and acquire a fibrous structure with a smaller diameter.<sup>40,41</sup> In addition, many studies have shown that cell proliferation and cell spreading in electrospun scaffolds could be enhanced by decreased fiber size.<sup>42,43</sup>

Changes in the surface topography of implantable materials, such as surface modification, porosity, roughness, and water contact angle, could affect cell adhesion, proliferation and migration by influencing actin cytoskeleton reorganization and filopodia formation through integrin receptor signaling.<sup>44,45</sup> Numerous physical and chemical properties of the biomaterial change after the addition of ATP. The surface roughness of electrospun nanomembranes is increased after incorporation with ATP, which may be changed by the unique rod-like or fibrous morphology of ATP crystals.<sup>46</sup> Molly M. Stevens' approach suggested that the enhanced nanoscale roughness of scaffolds could increase cell attachment,

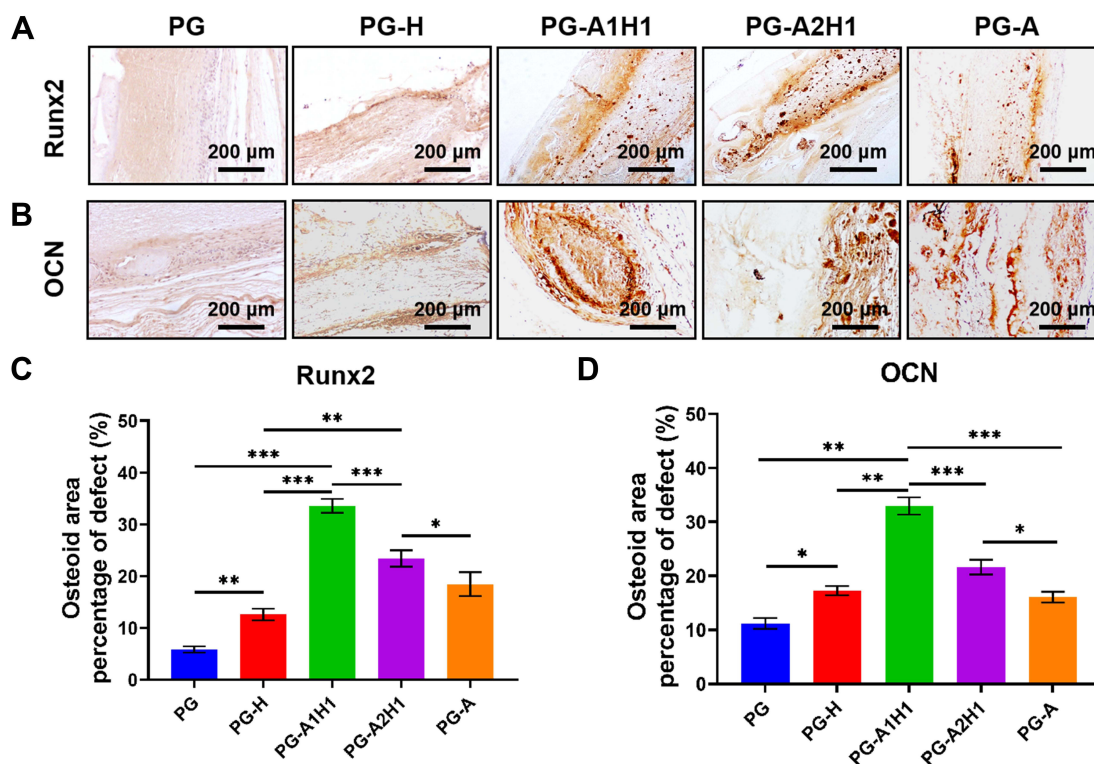


**Figure 7** Immunohistochemical staining after implantation of nanofibrous materials for 12 weeks. **(A)** Runx2. **(B)** OCN. **(C and D)** Quantitative analysis of protein expression from **(A and B)**. Data are shown as the mean  $\pm$  standard deviation ( $n = 3$ ). \* $p < 0.05$ , \*\* $p < 0.01$ , \*\*\* $p < 0.001$  between groups. Scale bar = 200  $\mu\text{m}$ . **Abbreviations:** Runx2, runt-related transcription factor 2; OCN, osteocalcin.

proliferation, and the expression of matrix components.<sup>47</sup> Meanwhile, the hydrophilicity presented by the water contact angle and swelling rate is improved, which could facilitate the adhesion and growth of BMSCs on the surface of the material.<sup>42</sup>

Nanofibrous sheets should have good toughness and adequate mechanical strength when applied to bone tissue implants to better match the host bone tissue defect. Our results showed that the tensile properties of the material were improved after adding attapulgite. The ideal BTE scaffold should be degradable, and the biodegradation rate should match the growth velocity of new bone tissue.<sup>13</sup> All of the groups degraded quickly in the first three weeks. The PG-A2H1 group had 84% of its initial mass at 6 weeks, while the PG group merely had approximately 78% of its initial mass remaining, which was the most mass loss among all the groups. In addition, the degradation rate of PG-A2H1 was slower than those of the other groups after the third week. Therefore, adding attapulgite can slow down the degradation of the biomaterial, and it will provide favorable mechanical support when the new bone tissue grows slowly.

In BTE, biocompatibility is essential to assess whether a material can provide a suitable microenvironment for cell survival, proliferation and differentiation.<sup>48</sup> The results of SEM, live/dead staining and cytoskeleton actin staining showed that the BMSCs grew well on the material, and the cytoskeleton spread well, indicating that the nanofiber membrane can provide a favorable microenvironment for cell growth. The CCK-8 results further showed excellent biocompatibility and cell proliferation function when ATP/HA was incorporated into the materials. Lucie Bacakova's study reported that the attachment of cells to the surface of biomaterials is mediated by extracellular or temporary matrix molecules such as fibronectin, vitronectin, collagen, laminin or fibrin.<sup>44</sup> Attapulgite has strong adsorption properties and can spontaneously adsorb bioactive molecules from body fluids and other body fluids to the material, which could build up a benign microenvironment for adherent cells. A series of consequences indicated that the material incorporating different ATP/HA ratios acquired favorable histocompatibility and could match the requirements of BTE scaffolds.

The ALP activity of BMSCs increased after seeding for 14 days, which indicated that PCL/GEL/ATP/HA nanofiber membranes could induce osteogenic responses in BMSCs in vitro. In addition, ARS staining showed that osteoblasts in

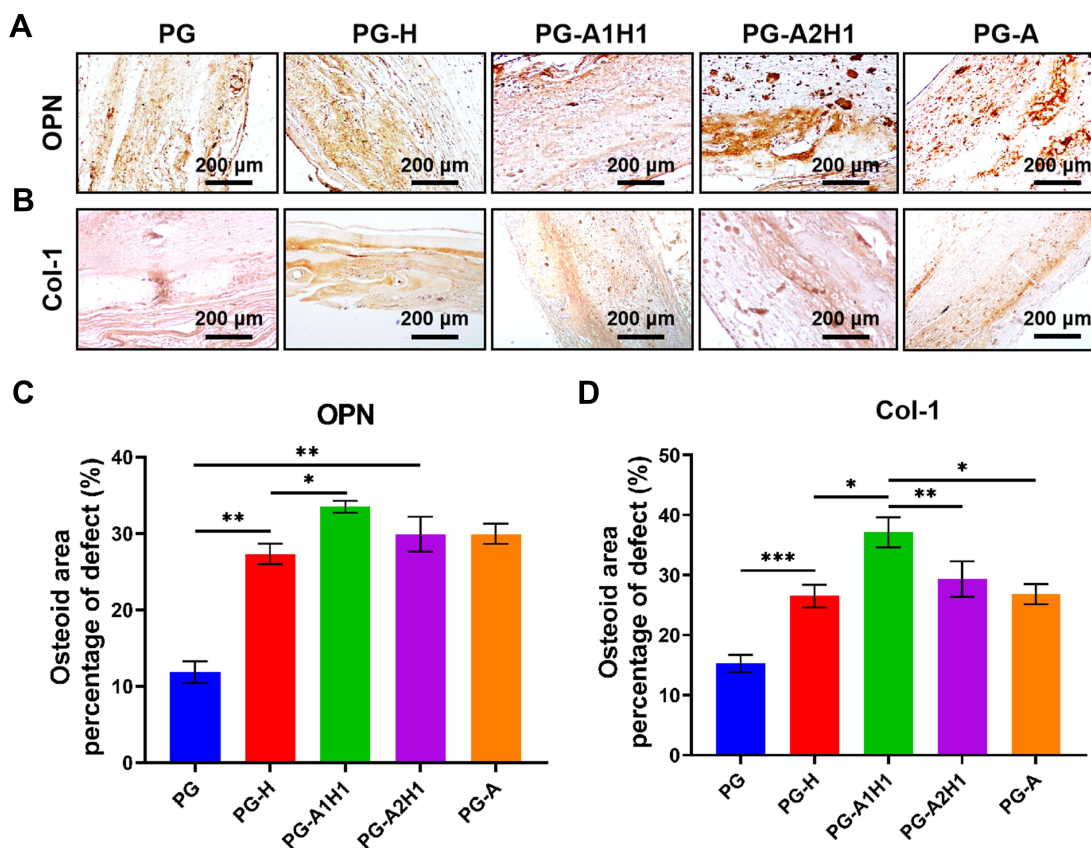


**Figure 8** Immunohistochemical staining results after implantation of nanofiber materials for 12 weeks. (A) OPN. (B) Col-1. (C and D) Quantitative analysis of protein expression from (A and B). Scale bar = 200 μm. Data are shown as the mean ± standard deviation (n = 3). Scale bar = 200 μm. \*p < 0.05, \*\*p < 0.01, \*\*\*p < 0.001. **Abbreviations:** OPN, osteopontin; Col-1, collagen type 1.

the PCL/GEL/ATP/HA group secreted significant extracellular calcium deposits compared with the groups without nano-ATP. These results indicate that the incorporation of nano-ATP can effectively induce the differentiation and mineralization of BMSCs due to ATP being rich in various ions, such as  $\text{Si}^{4+}$ ,  $\text{Ca}^{2+}$  and  $\text{Mg}^{2+}$ . Werner EG Müller's approach proved that biosilica can induce expanded biomineralization of SaOS-2 cells in vitro.<sup>49</sup>

The osteogenic expression levels of *ALP*, *OCN*, *OPN*, *Runx2*, *OSX* and other genes changed after mixing different contents of ATP/HA. As the proportion of attapulgite increased, the expression levels revealed that the osteogenic gene expression in the PG-A1H1 group and PG-A2H1 group was significantly improved. The specific mechanism by which attapulgite can promote the differentiation of BMSCs into osteoblasts is still unclear. Its osteoinductive effect is probably related to its silicon and magnesium contents. It has been reported that silicon and magnesium ions have osteoinductive effects.<sup>50,51</sup> Many studies have proven that silicon ions can improve the synthesis of type 1 collagen to enhance osteogenic differentiation, and a small amount of  $\text{Si}^{4+}$  also enhances synthetic apatite materials such as bioapatite and HA due to its stability and biological activity.<sup>52,53</sup>  $\text{Si}^{4+}$  can also induce the production of bone extracellular matrix (ECM) by enhancing prolyl-4-hydroxylase (prolyl-4-hydroxylase).<sup>34</sup> Magnesium ions also have a certain osteoinductive effect.<sup>54–58</sup> In addition, ATP has a large specific surface area and strong adsorption capacity and can absorb growth factors and nutrients in the surrounding tissues, which is beneficial for promoting the regeneration of defective tissues.<sup>33,59–61</sup> The physical and chemical properties and structural characteristics of ATP make it a potential material for bone tissue repair.<sup>33</sup> Our previous experiments confirmed that nanoattapulgite has good biocompatibility and promotes bone formation.<sup>62,63</sup>

The results of the rat skull defect model showed that a large amount of new bone tissue was observed in the groups that incorporated attapulgites at 12 weeks; furthermore, the PG-A1H1 and PG-A2H1 groups expressed more new bone than the control group. Immunohistological staining also indicated that the expression levels of *Runx2*, *Col-1*, *OCN* and

OPN in the A1H1 group and PG-A2H1 group were significantly better than those in the other groups. These results further confirmed that ATP is a substance that could exert synergetic effects with HA to enhance osteoinductive properties. Therefore, it may have broad application prospects in the field of BTE.

## Conclusion

Electrospinning technology is an effective method for preparing porous nanofiber membranes. In this study, we successfully fabricated nanofiber membranes containing different proportions of PCL/GEL/ATP/HA using electrospinning technology. Compared with materials without ATP, the composite nanomaterials showed good biocompatibility. In addition, ATP was able to produce a synergistic effect on bone formation. The histological staining results after 12 weeks further proved its synergistic effect. Therefore, the PCL/GEL/HA nanofiber membrane mixed with different proportions of ATP has a synergistic osteogenesis effect.

## Acknowledgments

This work was funded by the Key Project of Science and Technology of Jiangsu Province (Grant BE2018644).

## Disclosure

The authors declare no conflicts of interest.

## References

1. Zhang L, Yang G, Johnson BN, Jia X. Three-dimensional (3D) printed scaffold and material selection for bone repair. *Acta Biomater.* 2019;84:16–33. doi:10.1016/j.actbio.2018.11.039
2. Yang YP, Labus KM, Gadowski BC, et al. Osteoinductive 3D printed scaffold healed 5 cm segmental bone defects in the ovine metatarsus. *Sci Rep.* 2021;11(1):6704. doi:10.1038/s41598-021-86210-5
3. Roseti L, Parisi V, Petretta M, et al. Scaffolds for bone tissue engineering: state of the art and new perspectives. *Mater Sci Eng C Mater Biol Appl.* 2017;78:1246–1262. doi:10.1016/j.msec.2017.05.017
4. Jin S, Xia X, Huang J, et al. Recent advances in PLGA-based biomaterials for bone tissue regeneration. *Acta Biomater.* 2021;127:56–79. doi:10.1016/j.actbio.2021.03.067
5. Chen X, Zhu L, Wen W, Lu L, Luo B, Zhou C. Biomimetic mineralisation of eggshell membrane featuring natural nanofiber network structure for improving its osteogenic activity. *Colloids Surf B Biointerfaces.* 2019;179:299–308. doi:10.1016/j.colsurfb.2019.04.009
6. Kim HD, Amirthalingam S, Kim SL, Lee SS, Rangasamy J, Hwang NS. Biomimetic materials and fabrication approaches for bone tissue engineering. *Adv Healthcare Mater.* 2017;6(23):1700612. doi:10.1002/adhm.201700612
7. Lee J, Byun H, Madhurakkat Perikamana SK, Lee S, Shin H. Current advances in immunomodulatory biomaterials for bone regeneration. *Adv Healthc Mater.* 2019;8(4):e1801106. doi:10.1002/adhm.201801106
8. Bedair TM, Heo Y, Ryu J, Bedair HM, Park W, Han DK. Biocompatible and functional inorganic magnesium ceramic particles for biomedical applications. *Biomater Sci.* 2021;9(6):1903–1923. doi:10.1039/D0BM01934H
9. Shirzaei Sani I, Rezaei M, Baradar Khoshfetrat A, Razzaghi D. Preparation and characterization of polycaprolactone/chitosan-g-polycaprolactone/hydroxyapatite electrospun nanocomposite scaffolds for bone tissue engineering. *Int J Biol Macromol.* 2021;182:1638–1649.
10. Wubneh A, Tsekoura EK, Ayranci C, Uludag H. Current state of fabrication technologies and materials for bone tissue engineering. *Acta Biomater.* 2018;80:1–30. doi:10.1016/j.actbio.2018.09.031
11. Alonzo M, Primo FA, Kumar SA, et al. Bone tissue engineering techniques, advances and scaffolds for treatment of bone defects. *Curr Opin Biomed Eng.* 2021;17. doi:10.1016/j.cobme.2020.100248
12. Zienkiewicz-Strzalka M, Derylo-Marczewska A, Skorik YA, Petrova VA, Choma A, Komaniecka I. Silver nanoparticles on chitosan/silica nanofibers: characterization and antibacterial activity. *Int J Mol Sci.* 2019;21:1. doi:10.3390/ijms21010166
13. Wang Z, Wang Y, Yan J, et al. Pharmaceutical electrospinning and 3D printing scaffold design for bone regeneration. *Adv Drug Deliv Rev.* 2021;174:504–534. doi:10.1016/j.addr.2021.05.007
14. Purohit SD, Bhaskar R, Singh H, Yadav I, Gupta MK, Mishra NC. Development of a nanocomposite scaffold of gelatin–alginate–graphene oxide for bone tissue engineering. *Int J Biol Macromol.* 2019;133:592–602. doi:10.1016/j.ijbiomac.2019.04.113
15. Lin W, Chen M, Qu T, Li J, Man Y. Three-dimensional electrospun nanofibrous scaffolds for bone tissue engineering. *J Biomed Mater Res B Appl Biomater.* 2020;108(4):1311–1321. doi:10.1002/jbm.b.34479
16. Jin S, Yang R, Chu C, et al. Topological structure of electrospun membrane regulates immune response, angiogenesis and bone regeneration. *Acta Biomater.* 2021;129:148–158. doi:10.1016/j.actbio.2021.05.042
17. Deuerling S, Kugler S, Klotz M, Zollfrank C, Van Opdenbosch D. A perspective on bio-mediated material structuring. *Adv Mater.* 2018;30(19):1703656. doi:10.1002/adma.201703656
18. Elkhoully H, Mamdouh W, El-Korashy DI. Electrospun nano-fibrous bilayer scaffold prepared from polycaprolactone/gelatin and bioactive glass for bone tissue engineering. *J Mater Sci Mater Med.* 2021;32:9. doi:10.1007/s10856-020-06479-2
19. Suo H, Zhang D, Yin J, Qian J, Wu ZL, Fu J. Interpenetrating polymer network hydrogels composed of chitosan and photocrosslinkable gelatin with enhanced mechanical properties for tissue engineering. *Mater Sci Eng.* 2018;92:612–620. doi:10.1016/j.msec.2018.07.016

20. Lo S, Fauzi MB. Current update of collagen nanomaterials—fabrication, characterisation and its applications: a review. *Pharmaceutics*. 2021;13(3):316. doi:10.3390/pharmaceutics13030316
21. Liu F, Liu Y, Sun Z, et al. Preparation and antibacterial properties of epsilon-polylysine-containing gelatin/chitosan nanofiber films. *Int J Biol Macromol*. 2020;164:3376–3387. doi:10.1016/j.ijbiomac.2020.08.152
22. Yao R, He J, Meng G, Jiang B, Wu F. Electrospun PCL/Gelatin composite fibrous scaffolds: mechanical properties and cellular responses. *J Biomater Sci Polym Ed*. 2016;27(9):824–838. doi:10.1080/09205063.2016.1160560
23. Sharpe JM, Lee H, Hall AR, Bonin K, Guthold M. Mechanical properties of electrospun, blended fibrinogen: PCL nanofibers. *Nanomaterials*. 2020;10:9. doi:10.3390/nano10091843
24. Karimi-Soflou R, Mohseni-Vadeghani E, Karkhaneh A. Controlled release of resveratrol from a composite nanofibrous scaffold: effect of resveratrol on antioxidant activity and osteogenic differentiation. *J Biomed Mater Res A*. 2022;110(1):21–30. doi:10.1002/jbm.a.37262
25. Marins NH, Lee BEJ, e Silva RM, Raghavan A, Villarreal Carreño NL, Grandfield K. Niobium pentoxide and hydroxyapatite particle loaded electrospun polycaprolactone/gelatin membranes for bone tissue engineering. *Colloids Surf B Biointerfaces*. 2019;182:110386. doi:10.1016/j.colsurfb.2019.110386
26. Ribeiro N, Sousa A, Cunha-Reis C, et al. New prospects in skin regeneration and repair using nanophased hydroxyapatite embedded in collagen nanofibers. *Nanomedicine*. 2021;33:102353. doi:10.1016/j.nano.2020.102353
27. Liu W, Dong X, Qin H, Sui L, Wang J. Three-dimensional porous reduced graphene oxide/hydroxyapatite membrane for guided bone regeneration. *Colloids Surf B Biointerfaces*. 2021;208:112102. doi:10.1016/j.colsurfb.2021.112102
28. Liu Y, Dang Z, Wang Y, Huang J, Li H. Hydroxyapatite/graphene-nanosheet composite coatings deposited by vacuum cold spraying for biomedical applications: inherited nanostructures and enhanced properties. *Carbon*. 2014;67:250–259. doi:10.1016/j.carbon.2013.09.088
29. Lee JH, Shin YC, Lee SM, et al. Enhanced osteogenesis by reduced graphene oxide/hydroxyapatite nanocomposites. *Sci Rep*. 2015;5:18833. doi:10.1038/srep18833
30. Turhani D, Weissenböck M, Watzinger E, et al. In vitro study of adherent mandibular osteoblast-like cells on carrier materials. *Int J Oral Maxillofac Surg*. 2005;34(5):543–550. doi:10.1016/j.ijom.2004.10.023
31. Zhao H, Zhang X, Zhou D, et al. Collagen, polycaprolactone and attapulgite composite scaffolds for in vivo bone repair in rabbit models. *Biomed Mater*. 2020;15(4):045022. doi:10.1088/1748-605X/ab843f
32. Wang Z, Hui A, Zhao H, et al. A novel 3D-bioprinted porous nano attapulgite scaffolds with good performance for bone regeneration. *Int J Nanomedicine*. 2020;15:6945–6960. doi:10.2147/IJN.S254094
33. Wang W, Wang A. Recent progress in dispersion of palygorskite crystal bundles for nanocomposites. *Appl Clay Sci*. 2016;119:18–30. doi:10.1016/j.clay.2015.06.030
34. Tamburaci S, Tihminlioglu F. Development of Si doped nano hydroxyapatite reinforced bilayer chitosan nanocomposite barrier membranes for guided bone regeneration. *Mater Sci Eng C Mater Biol Appl*. 2021;128:112298. doi:10.1016/j.msec.2021.112298
35. Tsai SW, Huang SS, Yu WX, Hsu YW, Hsu FY. Collagen scaffolds containing hydroxyapatite-CaO fiber fragments for bone tissue engineering. *Polymers*. 2020;12:5. doi:10.3390/polym12051174
36. Gu Y, Loh N, Kho K, Tor S, Cheang P. Spark plasma sintering of hydroxyapatite powders. *Biomaterials*. 2002;23(1):37–43. doi:10.1016/S0142-9612(01)00076-X
37. Saber-Samandari S, Gross KA. Amorphous calcium phosphate offers improved crack resistance: a design feature from nature? *Acta Biomater*. 2011;7(12):4235–4241. doi:10.1016/j.actbio.2011.06.048
38. Tsai SW, Yu WX, Hwang PA, et al. Fabrication and characterization of strontium-substituted hydroxyapatite-CaO-CaCO<sub>3</sub> nanofibers with a mesoporous structure as drug delivery carriers. *Pharmaceutics*. 2018;10:4. doi:10.3390/pharmaceutics10040179
39. Tsai SW, Hsu YW, Pan WL, Hsu FY. The effect of strontium-substituted hydroxyapatite nanofibrous matrix on osteoblast proliferation and differentiation. *Membranes*. 2021;11:8.
40. Son WK, Youk JH, Lee TS, Park WH. The effects of solution properties and polyelectrolyte on electrospinning of ultrafine poly(ethylene oxide) fibers. *Polymer*. 2004;45(9):2959–2966. doi:10.1016/j.polymer.2004.03.006
41. Gautam S, Dinda AK, Mishra NC. Fabrication and characterization of PCL/gelatin composite nanofibrous scaffold for tissue engineering applications by electrospinning method. *Mater Sci Eng*. 2013;33(3):1228–1235. doi:10.1016/j.msec.2012.12.015
42. Sadeghi A, Moztarzadeh F, Aghazadeh Mohandesi J. Investigating the effect of chitosan on hydrophilicity and bioactivity of conductive electrospun composite scaffold for neural tissue engineering. *Int J Biol Macromol*. 2019;121:625–632. doi:10.1016/j.ijbiomac.2018.10.022
43. Gnani S, Fornasari BE, Tonda-Turo C, et al. The influence of electrospun fiber size on Schwann cell behaviour and axonal outgrowth. *Mater Sci Eng C Mater Biol Appl*. 2015;48:620–631. doi:10.1016/j.msec.2014.12.055
44. Bacakova L, Filova E, Parizek M, Ruml T, Svorcik V. Modulation of cell adhesion, proliferation and differentiation on materials designed for body implants. *Biotechnol Adv*. 2011;29(6):739–767. doi:10.1016/j.biotechadv.2011.06.004
45. Harvey AG, Hill EW, Bayat A. Designing implant surface topography for improved biocompatibility. *Expert Rev Med Devices*. 2013;10(2):257–267. doi:10.1586/erd.12.82
46. Wang B, Sun Z, Sun Q, et al. The preparation of bifunctional electrospun air filtration membranes by introducing attapulgite for the efficient capturing of ultrafine PMs and hazardous heavy metal ions. *Environ Pollut*. 2019;249:851–859. doi:10.1016/j.envpol.2019.03.122
47. Stevens MM, George JH. Exploring and engineering the cell surface interface. *Science*. 2005;310(5751):1135–1138. doi:10.1126/science.1106587
48. Qian Y, Zhou X, Zhang F, Diekwisch TGH, Luan X, Yang J. Triple PLGA/PCL Scaffold Modification Including Silver Impregnation, Collagen Coating, and Electrospinning Significantly Improve Biocompatibility, Antimicrobial, and Osteogenic Properties for Orofacial Tissue Regeneration. *ACS Appl Mater Interfaces*. 2019;11(41):37381–37396. doi:10.1021/acsami.9b07053
49. Muller WE, Tolba E, Schroder HC, Diehl-Seifert B, Link T, Wang X. Biosilica-loaded poly(-caprolactone) nanofibers mats provide a morphogenetically active surface scaffold for the growth and mineralization of the osteoclast-related SaOS-2 cells. *Biotechnol J*. 2014;9(10):1312–1321. doi:10.1002/biot.201400277
50. Pathmanapan S, Sekar M, Pandurangan A, Anandasadagopan S. Fabrication of mesoporous silica nanoparticle-incorporated coaxial nanofiber for evaluating the in vitro osteogenic potential. *Appl Biochem Biotechnol*. 2022;194(1):302–322. doi:10.1007/s12010-021-03741-3



51. Suryavanshi A, Khanna K, Sindhu KR, Bellare J, Srivastava R. Magnesium oxide nanoparticle-loaded polycaprolactone composite electrospun fiber scaffolds for bone-soft tissue engineering applications: in-vitro and in-vivo evaluation. *Biomed Mater.* 2017;12(5):055011. doi:10.1088/1748-605X/aa792b
52. Alshemary AZ, Akram M, Goh Y-F, et al. Synthesis, characterization, in vitro bioactivity and antimicrobial activity of magnesium and nickel doped silicate hydroxyapatite. *Ceram Int.* 2015;41(9):11886–11898. doi:10.1016/j.ceramint.2015.06.003
53. Patel N, Best SM, Bonfield W, et al. A comparative study on the in vivo behavior of hydroxyapatite and silicon substituted hydroxyapatite granules. *J Mater Sci Mater Med.* 2002;13(12):1199–1206. doi:10.1023/A:1021114710076
54. Behera M, Rajput M, Acharya S, Nadammal N, Suwas S, Chatterjee K. Zinc and cerium synergistically enhance the mechanical properties, corrosion resistance, and osteogenic activity of magnesium as resorbable biomaterials. *Biomed Mater.* 2021;16:4. doi:10.1088/1748-605X/ac0453
55. Luo R, Huang Y, Yuan X, et al. Controlled co-delivery system of magnesium and lanthanum ions for vascularized bone regeneration. *Biomed Mater.* 2021;16:6. doi:10.1088/1748-605X/ac2886
56. Yuan Z, Wei P, Huang Y, et al. Injectable PLGA microspheres with tunable magnesium ion release for promoting bone regeneration. *Acta Biomater.* 2019;85:294–309. doi:10.1016/j.actbio.2018.12.017
57. Lin Z, Wu J, Qiao W, et al. Precisely controlled delivery of magnesium ions thru sponge-like monodisperse PLGA/nano-MgO-alginate core-shell microsphere device to enable in-situ bone regeneration. *Biomaterials.* 2018;174:1–16. doi:10.1016/j.biomaterials.2018.05.011
58. Wang Q, Xu L, Willumeit-Römer R, Luthringer-Feyerabend BJC. Macrophage-derived oncostatin M/bone morphogenetic protein 6 in response to Mg-based materials influences pro-osteogenic activity of human umbilical cord perivascular cells. *Acta Biomater.* 2021;133:268–279. doi:10.1016/j.actbio.2020.12.016
59. Ha W, Wang ZH, Zhao XB, Shi YP. Reinforced supramolecular hydrogels from attapulgite and cyclodextrin pseudopolyrotaxane for sustained intra-articular drug delivery. *Macromol Biosci.* 2021;21(1):e2000299. doi:10.1002/mabi.202000299
60. Teng Y, Jiang Z, Yu A, Yu H, Huang Z, Zou L. Optimization of preparation parameters for environmentally friendly attapulgite functionalized by chitosan and its adsorption properties for Cd(2). *Environ Sci Pollut Res Int.* 2021;28(32):44064–44078. doi:10.1007/s11356-021-13788-8
61. Ji J, Xie W. Removal of aflatoxin B(1) from contaminated peanut oils using magnetic attapulgite. *Food Chem.* 2021;339:128072. doi:10.1016/j.foodchem.2020.128072
62. Ning Y, Qin W, Ren Y, Li C, Chen W, Zhao H. [Effect of icariin/attapulgite/collagen type I/polycaprolactone composite scaffold in repair of rabbit tibia defect]. *Zhongguo xiu fu chong jian wai ke za zhi.* 2019;33(9):1181–1189. Chinese. doi:10.7507/1002-1892.201902044
63. Zhang XM, Wang SY, Li G, Zhao HB. The study of osteogenic induction of type I Collagen/Poly (caprolactone)/attapulgite composite scaffold materials in vitro. *Chin Biotechnol.* 2016;36(5):27–33.

International Journal of Nanomedicine

Dovepress

## Publish your work in this journal

The International Journal of Nanomedicine is an international, peer-reviewed journal focusing on the application of nanotechnology in diagnostics, therapeutics, and drug delivery systems throughout the biomedical field. This journal is indexed on PubMed Central, MedLine, CAS, SciSearch®, Current Contents®/Clinical Medicine, Journal Citation Reports/Science Edition, EMBase, Scopus and the Elsevier Bibliographic databases. The manuscript management system is completely online and includes a very quick and fair peer-review system, which is all easy to use. Visit <http://www.dovepress.com/testimonials.php> to read real quotes from published authors.

Submit your manuscript here: <https://www.dovepress.com/international-journal-of-nanomedicine-journal>